Food Biophysics (2022) 17:181–197
https://doi.org/10.1007/s11483-021-09707-6

ORIGINAL ARTICLE

The melting properties of D-α-glucose, D-β-fructose, D-sucrose, D-α-galactose, and D-α-xylose and their solubility in water: A revision

Yeong Zen Chua[1,2] · Hoang Tam Do[3] · Aarti Kumar[3] · Moritz Hallermann[3] · Dzmitry Zaitsau[2,4] · Christoph Schick[1,2,5] · Christoph Held[3]

Received: 28 October 2021 / Accepted: 30 November 2021 / Published online: 28 December 2021

Abstract

Saccharides are still commonly isolated from biological feedstock by crystallization from aqueous solutions. Precise thermodynamic data on solubility are essential to optimize the downstream crystallization process. Solubility modeling, in turn, requires knowledge of melting properties. In the first part of this work, following our previous work on amino acids and peptides, D-α-glucose, D-β-fructose, D-sucrose, D-α-galactose, and D-α-xylose were investigated with Fast Scanning Calorimetry (FSC) in a wide scanning rate range (2000 $K \cdot s^{-1}$ to 10000 $K \cdot s^{-1}$). Using the experimental melting properties of saccharides from FSC allowed successfully modeling aqueous solubility for D-sucrose and D-α-galactose with the equation of state PC-SAFT. This provides cross-validation of the measurement methods to determine accurate experimental melting properties with FSC. Unexpectedly, the experimental FSC melting temperatures, extrapolated to zero scanning rates for thermal lag correction, were higher than results determined with DSC and available literature data. To clarify this inconsistency, FSC measurements towards low scanning rates from 10000 $K \cdot s^{-1}$ to 1 $K \cdot s^{-1}$ (D-α-glucose, D-β-fructose, D-sucrose) overlapping with the scanning rates of DSC and literature data were combined. At scanning rates below 1000 $K \cdot s^{-1}$, the melting properties followed a consistent non-linear trend, observed in both the FSC and the literature data. In order to understand the non-linear decrease of apparent melting temperatures with decreasing heating rate, the endothermic peaks were investigated in terms of isoconversional kinetics. The activation energies in the non-linear dependency region are in the range of $300 < E_A < 600 kJ \bullet mol^{-1}$. These values are higher than the enthalpy of sublimation for D-α-glucose, indicating that the non-linear behavior does not have a physical nature but attributes to chemical processes corresponding to the decomposition of molecular compounds within the crystal lattice before melting. The melting properties reported in the literature, commonly determined with conventional methods such as DSC, lead to inaccurate results due to the decomposition of these biomolecules at low heating rates. In addition, the FSC results at lower scanning rates coincide with results from DSC and literature in the overlapping scanning rate range, further validating the accuracy of FSC measurements to determine reliable melting properties of thermally labile biomolecules. The experimental FSC melting properties determined at higher scanning rates are considered as the correct equilibrium melting properties, which are not influenced by any chemical processes. The combination of FSC and PC-SAFT opens the door to model solubility of solid compounds that commonly decompose before melting.

Keywords Saccharides · Melting enthalpy · Melting temperature · Thermodynamics · Solubility · Solid–liquid equilibrium · PXRD · FSC · PC-SAFT

Introduction

Saccharides, in general, are essential ingredients in foods, pharmaceutics, or cosmetics, and they are important for the food industry. The knowledge of phase equilibria of saccharide solutions is indispensable. Due to the high viscosity of saccharide solutions, the experimental effort for its determination is time-consuming and cost-intensive.

Yeong Zen Chua and Hoang Tam Do Shared first authors.

✉ Christoph Held
christoph.held@tu-dortmund.de

Extended author information available on the last page of the article

The modeling of phase equilibria via a thermodynamic model is highly desired. The solubility in water (D-α-glucose [1, 2], D-β-fructose [3, 4], D-sucrose [3, 5, 6], D-α-galactose[7], and D-α-xylose[1, 7]) or in ethanol–water mixtures (D-α-glucose [2, 8, 9], D-β-fructose [9, 10], and D-sucrose [9, 11, 12]) have been widely investigated because of their crucial importance for industrial processes. Most of the solubility studies are carried out using the gravimetric method. The melting temperature (as well as the boiling temperature) is often the decisive factor whether crystallization (distillation) from solution is the most suitable separation method since it characterizes the phase state of the solute/solvent under the given conditions. Incorrect melting temperatures can lead to the consequence that the wrong separation method could be chosen.

This is of high interest in the pharmaceutical industry, where the knowledge of the solubility of organic compounds in pure solvents and solvent mixtures determines the synthesis and purification processes [13–15]. Since experimental determination of solubility is time-consuming and cost-intensive, modeling of solubility behavior of organic compounds through thermodynamic models is desirable. For accurate solubility modeling of organic compounds, reliable physical properties such as melting properties are crucial.

Melting parameters, as thermodynamic properties, are essential for the fundamental understanding of the structure of compounds and corresponding materials. Generally, melting properties of thermally unstable biomolecules are inaccessible with conventional methods, e.g. Differential Scanning Calorimetry (DSC), due to chemical decomposition (degradation) [16].With the access to high scanning rates with Fast Scanning Calorimetry (FSC), thermodynamic properties such as melting properties can be directly measured, especially for biomolecules without decomposition [17, 18]. Recently, an experimental FSC method has been developed for the successful determination of the melting properties of amino acids [19, 20], peptides [21, 22], nucleobases [23, 24], bio-polymers [17, 18] and low molecular mass pharmaceuticals [25].

In this work, we continue our previous research and characterize the melting properties of D-α-glucose, D-β-fructose, D-sucrose, D-α-galactose, and D-α-xylose employing the established experimental FSC method [19, 21, 26]. The saccharides were measured with FSC in a wide range of scanning rates from 2000 $K \cdot s^{-1}$ to 10000 $K \cdot s^{-1}$, and the experimental melting properties, extrapolated to zero scanning rates for thermal lag correction, were used as an input for the thermodynamic modeling framework PC-SAFT to model the aqueous solubility of the saccharides. As a result, the solubilities of D-sucrose and D-α-galactose were successfully modeled and were found to be in good agreement with the experimentally determined data. This provides validation of the melting properties determination via the experimental FSC method.

The melting parameters of saccharides were widely studied before with conventional calorimetric techniques, e.g. DSC. Unexpectedly the experimental melting properties determined with FSC were higher than results determined with DSC and available literature data. Due to low heating rates of the order of K min^{-1}, degradation could not be excluded in these experiments, though most literature data neglected the influence of degradation [27–33]. This discrepancy of melting properties between FSC and DSC was first observed by Magon et al. in studying the melting of D-sucrose with FSC, where a much higher melting temperature was determined by FSC at 1000 K s^{-1} (470 K) compared to the value determined by DSC at 10 K min^{-1} (424 K) [33]. The discrepancy was, at that time, mainly attributed to thermal lag and superheating [33]. However, the FSC measured melting properties extrapolated to zero scanning rates for correction of the thermal lag were nevertheless still higher than the DSC results. Another study by Toda et al. on the melting kinetics of D-sucrose by FSC revealed a change from "chemically" initiated melting to a first-order melting transition with superheating [34].

This unexpected observation leads us to study further experimental melting properties of D-α-glucose, D-β-fructose, D-sucrose with the FSC technique in a broader scanning rate range from 1 $K \cdot s^{-1}$ to 10000 $K \cdot s^{-1}$. This extended scanning rate range provides an overlap between FSC and DSC, both remeasured and literature data. The FSC results were then analyzed in terms of isoconversional kinetics in order to explain the observed unexpected behavior.

Experimental

Materials and Reagents The saccharides, D-α-glucose, D-β-fructose, D-sucrose, D-α-galactose, and D-α-xylose, were purchased and used without further purification, listed in Table 1.

Differential Scanning Calorimetry (DSC) A Pyris 1 DSC (PerkinElmer, USA) connected to an intracooler 100PE

Table 1 Substances, suppliers, CAS numbers, and mass-specific purities of the reagents used within this work

Substances	Supplier	CAS no	Purity
D-α-glucose	Merck	50–99-7	≥ 98
D-β-fructose	Sigma-Aldrich	57–48-7	≥ 99
D-sucrose	Sigma-Aldrich	57–50-1	≥ 99.5
D-α-galactose	BioChemica	59–23-4	≥ 99
D-α-xylose	Sigma-Aldrich	58–86-6	≥ 99

(Huber, Germany) was utilized to characterize the thermal behavior of the saccharides D-α-glucose, D-β-fructose, D-sucrose, D-α-galactose, and D-α-xylose at low heating rates. The measurements were performed starting from 223 to 423 K, with a scanning rate $\beta = 10$ K•min^{-1} (0.16 K·s^{-1}), and under an inert atmosphere of dry nitrogen with dew point lower than 160 K. Heat flow and temperature determinations were verified with indium and benzoic acid following the procedure recommended by GEFTA [35].

Each DSC measurement was performed with three consecutive steps: (i) empty reference and sample pans (for asymmetry correction of DSC), (ii) empty reference pan and sample pan with sapphire (for calibration), and (iii) empty reference pan and sample pan with the sample [35]. Before step (iii), the sample was degassed in a vacuum chamber for 2 h at 323 K to remove any water or volatile impurities. For each sample, the DSC measurements were repeated two times to ensure reproducibility [36–38].

Fast Scanning Calorimetry (FSC) The melting properties of saccharides were determined with a Flash DSC1 fast scanning calorimeter (Mettler Toledo, Switzerland). First for D-α-glucose, D-β-fructose, D-sucrose, D-α-galactose and D-α-xylose in the scanning rate range from 2000 K•s^{-1} to 10,000 K•s^{-1}, and then for D-α-glucose, D-β-fructose, and D-sucrose in the extended scanning rate range down to 1 K•s^{-1}. For all measurements, the start temperature was 303 K. The small samples (< 100 ng) were placed on the thin film chip sensor UFS1 [39] and measured under an inert atmosphere of dry nitrogen with a flow rate of about 50 ml•min^{-1}. The FSC measurement method was similar to the previously detailed experimental method [17, 19, 40, 41]. After conditioning and correction of the UFS1 sensor, as requested by the manufacturer, temperature calibration was performed according to the GEFTA recommendation using indium, bismuth, and tin [35].

Experimental Procedures In Fig. 1, the temperature–time profiles for DSC (top) and FSC (bottom) measurements are shown. The temperature–time profiles can be divided into three stages: (i) first stage for sample mass determination, (ii) the second stage for sample melting, and (iii) the third stage for the determination of the glass transition temperature, heat capacity difference between liquid and solid (glass) phases, as well as possible mass losses.

For DSC measurements in the first "reference" stage, the sample was heated at 10 K/min in steps of 50 K and isotherms of 2 min between each step. The temperature range for reference scans was chosen to have reproducible heating and cooling cycles. The reproducibility between scans #1 and #3 indicates no mass loss in this temperature range due

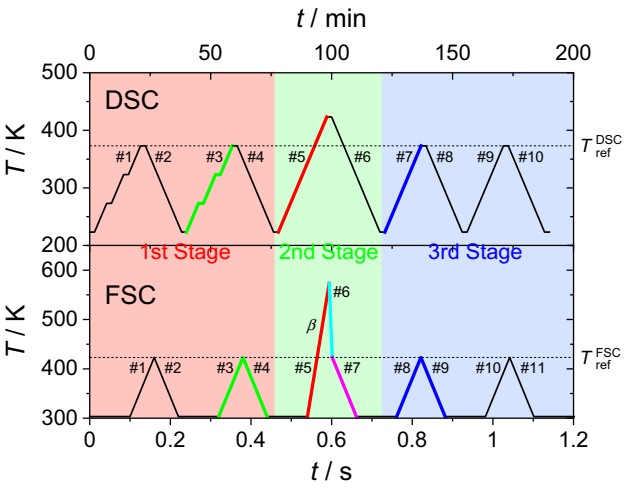

Fig. 1 Temperature–time profile for DSC (top) and FSC (bottom) measurements, consisting of three stages. 1st stage: sample mass determination (red segment), 2nd stage: sample melting (green segment), and 3rd stage: reheating of the supercooled sample (blue segment). The cooling segment #6 at 10,000 K•s^{-1} was added to reduce the time at high temperature and to avoid significant degradation, evaporation and sublimation

to sublimation or chemical transformations. In this stage, the specific heat capacity of the sample in the solid state was obtained and fitted linearly, allowing to extrapolate to higher temperatures, e.g. the melting temperature, according to

$$c^{S}_{p0i} = \left(a_{c^{S}_{p0i}} \bullet T\right) + b_{c^{S}_{p0i}} \quad (1)$$

where $a_{c^{S}_{p0i}}$ is the slope and $b_{c^{S}_{p0i}}$ is the intercept of the solid-state specific heat capacity function.

In the second stage, the sample was heated only slightly above the melting temperature to melt the sample fully and simultaneously minimize possible chemical degradation and sublimation/evaporation of the sample at high temperatures. If crystallization was avoided upon cooling the melted sample, the glass transition was determined in cooling segment #6 and the following heating and cooling cycles in the third stage.

For FSC measurements, a similar temperature–time profile as for the DSC measurements was used (Fig. 1) but on a totally different time scale (compare top and bottom time axis). After melting the sample (heating segment #5), the following cooling segment is subdivided into a cooling segment at the maximum possible cooling rate (#6, 10000 K•s^{-1}) followed by cooling at 500 K•s^{-1} (#7). This strategy effectively reduces chemical degradation and evaporation/sublimation of the sample at high temperatures and allows detection of the glass transition and the heat capacity of the deeply supercooled state from the first cooling scan (#7) [24].

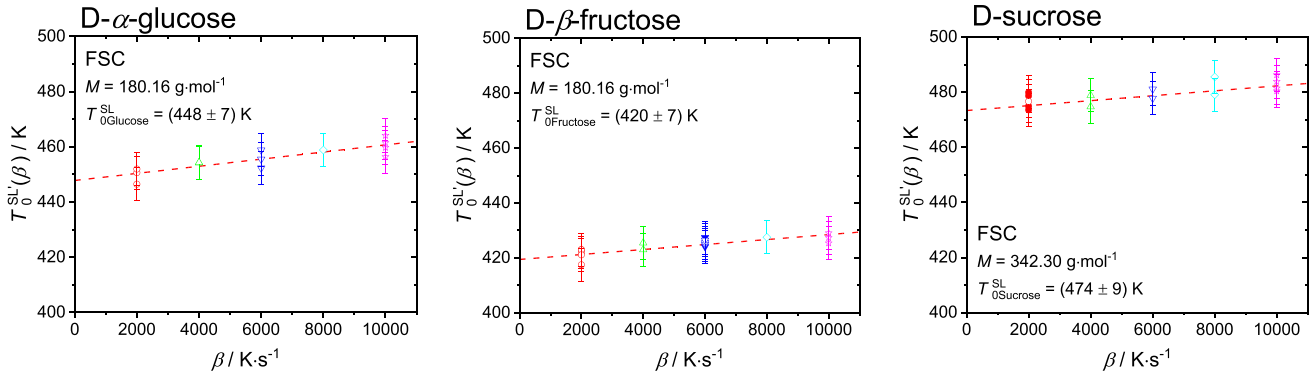

Fig. 2 Extrapolated onset temperature of the melting peak for (left) D-α-glucose, (middle) D-β-fructose and (right) D-sucrose as a function of heating rate. The melting temperature at zero heating rate is $T^{SL}_{0Glucose}$ = (448 ± 7) K, $T^{SL}_{0Fructose}$ = (420 ± 7) K and $T^{SL}_{0Sucrose}$ = (474 ± 9) K. The scanning rates used were 2000 K•s^{-1} (red circles), 4000 K•s^{-1} (green up-triangles), 6000 K•s^{-1} (blue down-triangles), 8000 K•s^{-1} (cyan diamonds), 10,000 K•s^{-1} (magenta stars). Solid symbols represent sample measurements without silicon oil, while empty symbols for sample measurements with silicon oil. The results for D-α-galactose and D-α-xylose are in Figure S3 in SI

As the samples measured in FSC were too small for direct determination of sample masses, the initial masses of the samples are determined as

$$m_0 = \frac{C^S_{p0i}[J \bullet K^{-1}]}{c^S_{p0i}[J \bullet g^{-1} \bullet K^{-1}]} \quad (2)$$

where C^S_{p0i} [J•K^{-1}] is the solid-state heat capacity determined in the first stage of the FSC measurements and c^S_{p0i} [J•g^{-1}•K^{-1}] is the specific heat capacity determined in DSC measurements at equal temperatures. For the first stage of the FSC measurements, the scanning rate of 500 K•s^{-1} was applied. The maximum temperature was chosen such that repeated heating and cooling cycles show reproducibility without sample mass loss due to sublimation or degradation. It was concluded in a previous work that determination of m_0 using Eq. (2) comes with an error of max. 11%, caused by FSC instrumental uncertainty and C^S_{p0i} measurements compared to literature[19].

Once the initial mass of the sample was determined, the melting properties (onset melting temperature, T^{SL}_{0i} and specific melting enthalpy, Δh^{SL}_{0i}) were determined in the heating step #5 in the second stage, as

$$\Delta h^{SL}_{0i} = \frac{\Delta H^{SL}_{0i} \bullet M}{m_0} \quad (3)$$

where the enthalpy change, ΔH^{SL}_{0i}, is the peak area from the heat-flow curve in heating step #5 and M is the molar mass. The specific melting enthalpy,Δh^{SL}_{0i}, is determined from the slope of the sample mass dependency of ΔH^{SL}_{0i}; for details, see Fig. 4 and references [22, 23, 41]. In order to ensure good thermal contact between the sample and the sensor

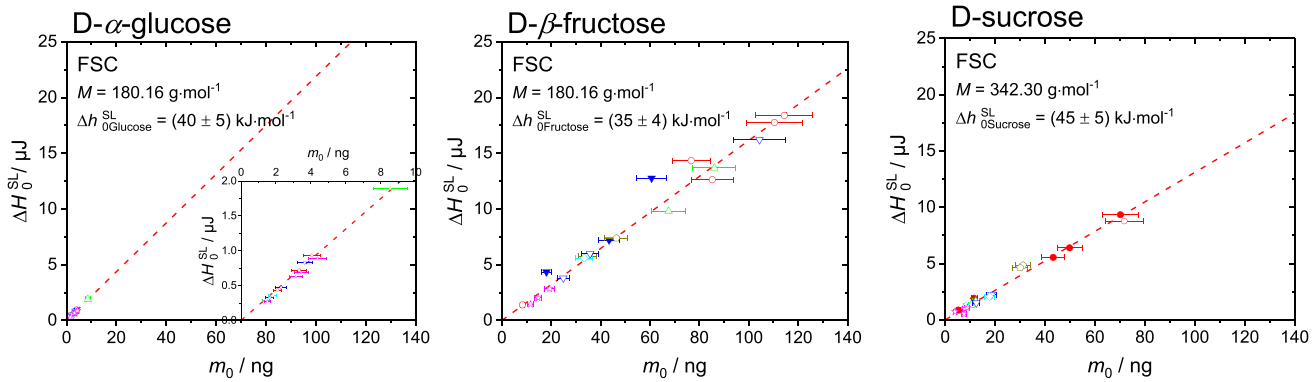

Fig. 3 Enthalpy for (left) D-α-glucose, (middle) D-β-fructose and (right) D-sucrose in respect to initial sample mass. The slope of the linear fits through zero origin was denoted as melting enthalpy, with $\Delta h^{SL}_{0Glucose}$ = (40 ± 5) kJ•mol^{-1}, $\Delta h^{SL}_{0Fructose}$ = (35 ± 4) kJ•mol^{-1}, $\Delta h^{SL}_{0Sucrose}$ = (45 ± 5) kJ•mol^{-1}. The symbols used were as described in Fig. 2. The results for D-α-galactose and D-α-xylose are in Figure S3 in SI

Table 2 Experimental melting properties (T_{0i}^{SL} and Δh_{0i}^{SL}) and glass transition temperature (T_{0i}^{G}), as well as heat capacity difference between liquid and solid states at the glass transition temperature ($\Delta c_{p0i}^{SL}(T_{0i}^{G})$) and at melting temperature ($\Delta c_{p0i}^{SL}(T_{0i}^{SL})$) of D-α-glucose, D-β-fructose, D-sucrose, D-α-galactose, and D-α-xylose measured with FSC

Substances	M	FSC								
		T_{0i}^{SL}	Δh_{0i}^{SL}	T_{0i}^{G}	$\Delta c_{p0i}^{SL}(T_{0i}^{G})$	$\Delta c_{p0i}^{SL}(T_{0i}^{SL})$	$a_{c_{p0i}^{S}}$	$b_{c_{p0i}^{S}}$	$a_{c_{p0i}^{L}}$	$b_{c_{p0i}^{L}}$
	/ g·mol^{-1}	/ K	/ kJ·mol^{-1}	/ K	/ J·mol^{-1}·K^{-1}	/ J·mol^{-1}·K^{-1}	/ J·mol^{-1}·K^{-2}	/ J·mol^{-1}·K^{-1}	/ J·mol^{-1}·K^{-2}	/ J·mol^{-1}·K^{-1}
D-α-glucose	180.16	448 ± 7	40 ± 5	324 ± 6	135 ± 10	115 ± 10	0.728	6.3	0.568	192.3
D-β-fructose	180.16	420 ± 7	35 ± 4	297 ± 4	158 ± 5	129 ± 5	0.757	3.5	0.523	230.3
D-sucrose	342.30	474 ± 9	45 ± 5	362 ± 1	231 ± 4	192 ± 4	1.517	-27.5	1.168	329.0
D-α-galactose	180.16	488 ± 7	47 ± 6	300 ± 2	135 ± 2	122 ± 2	0.750	-4.2	0.680	151.8
D-α-xylose	150.13	460 ± 7	42 ± 5	287 ± 4	114 ± 8	110 ± 8	0.598	4.2	0.582	125.2

Table 3 Experimental "*melting*" properties ($T_{0i}^{SL}(\beta)$ and Δh_{0i}^{SL}) and glass transition temperature (T_{0i}^{G}), as well as heat capacity difference between liquid and solid states at the glass transition temperature ($\Delta c_{p0i}^{SL}(T_{0i}^{G})$) and at melting temperature ($\Delta c_{p0i}^{SL}(T_{0i}^{SL})$) of D-α-glucose, D-β-fructose, D-sucrose, D-α-galactose, and D-α-xylose measured with DSC at 10 K min^{-1}

Substances	M	DSC								
		$T_{0i}^{SL}(\approx)$	Δh_{0i}^{SL}	T_{0i}^{G}	$\Delta c_{p0i}^{SL}(T_{0i}^{G})$	$\Delta c_{p0i}^{SL}(T_{0i}^{SL})$	$a_{c_{p0i}^{S}}$	$b_{c_{p0i}^{S}}$	$a_{c_{p0i}^{L}}$	$b_{c_{p0i}^{L}}$
	/ g·mol^{-1}	/ K	/ kJ·mol^{-1}	/ K	/ J·mol^{-1}·K^{-1}	/ J·mol^{-1}·K^{-1}	/ J·mol^{-1}·K^{-2}	/ J·mol^{-1}·K^{-1}	/ J·mol^{-1}·K^{-2}	/ J·mol^{-1}·K^{-1}
D-α-glucose	180.16	432 ± 1	36 ± 1	307 ± 2	154 ± 2	153 ± 2	0.728	6.3	0.716	164.0
D-β-fructose	180.16	382 ± 2	34 ± 1	286 ± 2	158 ± 8	154 ± 8	0.757	3.5	0.718	172.3
D-sucrose	342.30	459 ± 4	43 ± 2	330 ± 2	255 ± 4	225 ± 4	1.517	-27.5	0.122	303.1
D-α-galactose	180.16	441 ± 2	44 ± 2	303 ± 2	144 ± 2	141 ± 2	0.750	-4.2	0.728	145.5
D-α-xylose	150.13	427 ± 2	35 ± 2	281 ± 2	130 ± 2	118 ± 2	0.598	4.2	0.521	154.7

surface and to minimize sublimation/evaporation, the sample can be covered with silicon oil before heating step #5.

Due to the possible decomposition of the saccharides, the melting temperaturewas determined at relatively high heating rates. The peak-onset melting temperature $T_{0i}^{SL'}(\beta)$ of the endothermic melting peak was measured using heating rates from 2000 K•s^{-1} to 10000 K•s^{-1}. The equilibrium, thermal lag corrected melting temperatures T_{0i}^{SL} were determined by linear extrapolation of $T_{0i}^{SL'}(\beta)$ to heating rate $\beta = 0$ K•s^{-1} [35].

The specific heat capacities of the melted sample in the second stage and the liquid state above the glass transition in the third stage were jointly fitted to a linear function. The linear equation of the specific heat capacity of the liquid state is

$$c_{p0i}^{L} = \left(a_{c_{p0i}^{L}} \bullet T\right) + b_{c_{p0i}^{L}} \tag{4}$$

where $a_{c_{p0i}^{L}}$ is the slope and $b_{c_{p0i}^{L}}$ is the intercept of the liquid state specific heat capacity function.

For the determination of the glass transition temperature, only samples not covered with silicon oil were utilized. After melting, the samples were quenched rapidly at 10000 K•s^{-1} to reduce evaporation or crystallization. In the third stage, the melted sample was reheated to determine the parameters of the glass transition. The specific heat capacity of the liquid state above the glass transition from the third stage and the liquid heat capacity from the second stage, step #7, were jointly fitted linearly.

Solubility Modeling with PC-SAFT The melting properties determined experimentally with FSC in this work were applied in an equilibrium framework to model solubility of saccharide in water. Assuming a pure solid phase, the mole-fraction based solubility x_i^L can thus be calculated according to Prausnitz [42] as

$$\ln\left(x_i^L \bullet \gamma_i^L\right) = \frac{\Delta h_{0i}^{SL}}{R \bullet T_{0i}^{SL}}\left(1 - \frac{T_{0i}^{SL}}{T}\right) - \frac{1}{R \bullet T}\int_{T_{0i}^{SL}}^{T} \Delta c_{p0i}^{SL}(T)dT + \frac{1}{R}\int_{T_{0i}^{SL}}^{T} \frac{\Delta c_{p0i}^{SL}(T)}{T}dT \tag{5}$$

$$\Delta c_{p0i}^{SL}(T) = \left(a_{c_{p0i}^{L}} - a_{c_{p0i}^{S}}\right) \bullet T + \left(b_{c_{p0i}^{L}} - b_{c_{p0i}^{S}}\right) \tag{6}$$

with γ_i^L as the activity coefficient of the saccharide, R the universal gas constant, Δh_{0i}^{SL} the melting enthalpy at melting temperature and T_{0i}^{SL} the melting temperature. The $\Delta c_{p0i}^{SL}(T)$ is the temperature-dependent difference between the heat capacities in liquid (L) and solid (S) state of a pure saccharide determined from Eq. (6), where $a_{c_{p0i}^{L}}$ ($a_{c_{p0i}^{S}}$) and $b_{c_{p0i}^{L}}$ ($b_{c_{p0i}^{S}}$) as the slope and the intercept of the heat capacities from Eq. (1) and (4), respectively.

The detailed PC-SAFT description is provided in the Supplementary Information (SI). The PC-SAFT pure-component parameters used for the saccharides are already published in the literature [4]. The pure-component parameters were fitted to non-solubility properties such as osmotic coefficient and mixture density data in water at $T = 298.15$K using parameters in Table S1 in the SI. The diagrams of the fitted osmotic coefficients and mixture densities are shown in Figure S1 – S2 in the SI. The PC-SAFT pure-component parameters, as well as binary interaction parameters for the dispersion energy between the saccharide and water as used in this work, are listed in Table S1 in SI.

By analyzing Eq. (5) it can be seen that the melting parameters differently influence the solubility. An increase of Δh_{0i}^{SL} and T_{0i}^{SL} leads to a decrease of solubility while simultaneously an increase in T_{0i}^{SL} and $\Delta c_{p0i}^{SL}(T)$ will change the solubility-temperature curve to lesser temperature dependency. The influence of the solvent is taken into account with γ_i^L, which describes the interactions between the saccharide and the solvent in the liquid phase.

Additionally, the isothermal method with excess of the solute was applied to determine the aqueoues solubility and examine the crystal structure of the solid deposit in equilibrium with the saturated solutions at $T = 298.15$K and $T = 323.15$K. The crystal structure of the solid phase was measured by Powder X-Ray Diffraction (PXRD). The solubility model based on Eq. (5) and (6) requires that the crystal structure of the pure compound and the solid compound in the equilibrium state do not change during the solubility measurement.

Results

Melting properties with FSC. Following the experimental FSC method established in our previous research and characterization of melting properties of amino acids and peptides [19–22], the saccharides D-α-glucose, D-β-fructose, D-sucrose, D-α-galactose, and D-α-xylose were characterized experimentally with Fast Scanning Calorimetry (FSC) with scanning rates from 2000 K•s^{-1} to 10,000 K•s^{-1}. The onset temperatures, $T_{0i}^{SL'}(\beta)$, from the melting peak in heating step #5 with respect to heating rates, β, were shown in Fig. 2, while the enthalpy, ΔH_{0i}^{SL}, determined from the areas under the melting peaks with respect to sample mass were shown in Fig. 3.

In order to correct for the thermal lag and possible superheating due to the high scanning rates, the onset temperatures were extrapolated to zero scanning rate to obtain the equilibrium melting temperature, T_{0i}^{SL}. The enthalpy, ΔH_{0i}^{SL}, depends linearly on sample mass, m_0, independent of the scanning rates, and the slope from the linear dependency depicts the specific melting enthalpy, Δh_{0i}^{SL}. The glass transition temperature T_{0i}^{G} corresponds to the half-step temperature of the heat capacity step.

The melting properties (T_{0i}^{SL} and Δh_{0i}^{SL}) and glass transition temperature (T_{0i}^{G}), as well as heat capacity difference between liquid and solid states at the glass transition temperature ($\Delta c_{p0i}^{SL}(T_{0i}^{G})$) and at melting temperature ($\Delta c_{p0i}^{SL}(T_{0i}^{SL})$) measured with FSC were listed in Table 2.

The experimental melting properties determined from FSC (Table 2) and DSC (Table 3) showed a considerable discrepancy. In order to understand this discrepancy, further measurements with an extension of the scanning rates of FSC to lower values, ranging from 1000 K•s^{-1} down to 1 K•s^{-1}, were performed for D-α-glucose, D-β-fructose, and D-sucrose. The obtained data were compared to the DSC and literature data, cf. Table 4.

Melting Properties with DSC The saccharides D-α-glucose, D-β-fructose, D-sucrose, D-α-galactose and D-α-xylose were characterized experimentally with Differential Scanning Calorimetry (DSC) with the scanning rate 10 K•min^{-1}, presented in Fig. 4. The "*melting*" properties ($T_{0i}^{SL}(\beta)$ and Δh_{0i}^{SL}) and glass transition temperature (T_{0i}^{G}), as well as the heat capacity difference between liquid and solid states at the glass transition temperature ($\Delta c_{p0i}^{SL}(T_{0i}^{G})$) and at melting temperature ($\Delta c_{p0i}^{SL}(T_{0i}^{SL})$) measured with DSC were listed in Table 3.

FSC Scanning Rate Dependency Extended to Lower Values Scanning rate dependent measurements were conducted for D-α-glucose, D-β-fructose, and D-sucrose. The scanning rates of FSC were extended to lower values, ranging from 1000 K•s^{-1} to 1 K•s^{-1}, for comparison with results from DSC at 10 K•min^{-1} (0.17 K•s^{-1})and literature data [27, 31–34, 47–49].

In Fig. 5, the melting peak onset temperatures, determined with FSC for scanning rates from 10,000 K•s^{-1} to 1 K•s^{-1}, were presented as solid red circles together with the data from Fig. 2. The results at scanning rates below 10 K•s^{-1} are consistent with DSC and literature data (Fig. 5(inset)). The observed scanning rate dependency is strongly non-linear at low scanning rates, indicating other influences than thermal lag.

As in Figs. 2 and 5, the equilibrium melting temperature, T_{0i}^{SL}, was determined from FSC data for heating rates above 1000 K· s^{-1} as linear extrapolation of onset temperatures to zero scanning rate. This linear extrapolation as a correction for the thermal lag is shown as the dashed black line in Fig. 5. On the other hand, the onset temperatures decrease exponentially with decreasing scanning rates below 10 K•s^{-1}. The reported melting temperatures in the literature were obtained or extrapolated to zero scanning rate by using data from the scanning rate range showing the non-linear decrease of onset temperatures [27, 31–34, 47–49].

As in Fig. 3, the melting enthalpy, Δh_{0i}^{SL}, was determined from FSC as the slope of a linear fit (red dashed line) of enthalpy, ΔH_{0i}^{SL}, in respect to sample mass, m_0, regardless of the scanning rates, and fixing the origin to zero. The FSC melting enthalpy was depicted as the solid horizontal red line in Fig. 6, independent of the scanning rate. However, melting enthalpy determined from DSC and literature data have values lower than that determined by FSC. Furthermore, they exhibit a non-linear decrease with decreasing scanning rate below 10 K•s^{-1}.

Similar to the melting temperatures from the literature, the melting enthalpies reported in the literature were partly obtained at zero scanning rate by extrapolating the non-linear decreasing values [27, 31–34, 47–49]. This discrepancies of melting properties determined from FSC and literature data are presented in Table 4.

Activation Energy As shown in Figs. 5 and 6, depending on the scanning rate, the determined melting properties can be divided into two groups: A linear dependency for heating rates above 1000 K·s^{-1} and a non-linear dependency for heating rates below 1000 K·s^{-1}. The linear dependency can be described in terms of thermal lag due to limited heat transfer between the sensor membrane and the sample. The thermal lag increases with increasing scanning rate, which is corrected by linear extrapolations to zero scanning rate. We should note the investigation of D-sucrose melting by Toda et al. [34], where the temperature shift of the endothermic peak onset was evaluated in terms of a superposition of three phenomena: thermal lag, crystal superheating, and chemical decomposition. From our perspective, introducing the superheating phenomenon into consideration for crystals of molecular compounds is not necessarily needed, even of interest for understanding the melting process itself. It also should be mentioned that superheating should result in a non-linear behavior at high heating rates. In Fig. 5 a non-linear behavior is only seen for low heating rates. Therefore there is no need to consider superheating for the interpretation of our data. Furthermore, possible chemical decomposition at slow heating is nicely fitted with n-order kinetical equations (often 1st order). In this case, fitting the onset melting temperature against $\beta^{0.4–0.5}$ does not allow for distinguishing chemical decomposition and possible superheating. Therefore, we analyzed the observed dependence of onset

Table 4 Melting properties of D-α-glucose, D-β-fructose, and D-sucrose determined with FSC, DSC at 10 K·min^{-1} and from literature for comparison

Substances	T_{0i}^{SL}(≠)/ K		Δh_{0i}^{SL}/ kJ·mol^{-1}		
	β = 10 K·min^{-1}	β → 0	β = 10 K·min^{-1}	β → 0	
D-α-glucose		448 ± 7		40 ± 5	FSC
	432 ± 1		36 ± 1		DSC
	429.8	412.0	36.6	31.5	Ref. [32]
	428.4	419.7	35.1	33.4	Ref. [27]
		408.2		32.5	Ref. [48]
		416.2		32.3	Ref. [49]
	431.6				Ref. [47]
D-β-fructose		420 ± 7		35 ± 4	FSC
	382 ± 2		34 ± 1		DSC
	385.4	370.0	35.0	30.3	Ref. [31]
	398.9	385.9	31.9	27.8	Ref. [27]
		353.2		32.5	Ref. [48]
		381.2		30.5	Ref. [49]
	386.8				Ref. [47]
D-sucrose		474 ± 9		45 ± 5	FSC
	459 ± 4		43 ± 2		DSC
	457.2	424.4	45.0	32.0	Ref. [33]
	460.0	462.1			Ref. [34]
	462.1	457.7	43.3	24.5	Ref. [27]
		433.2		41.1	Ref. [48]
		446.2		40.4	Ref. [49]
	424.2				Ref. [47]

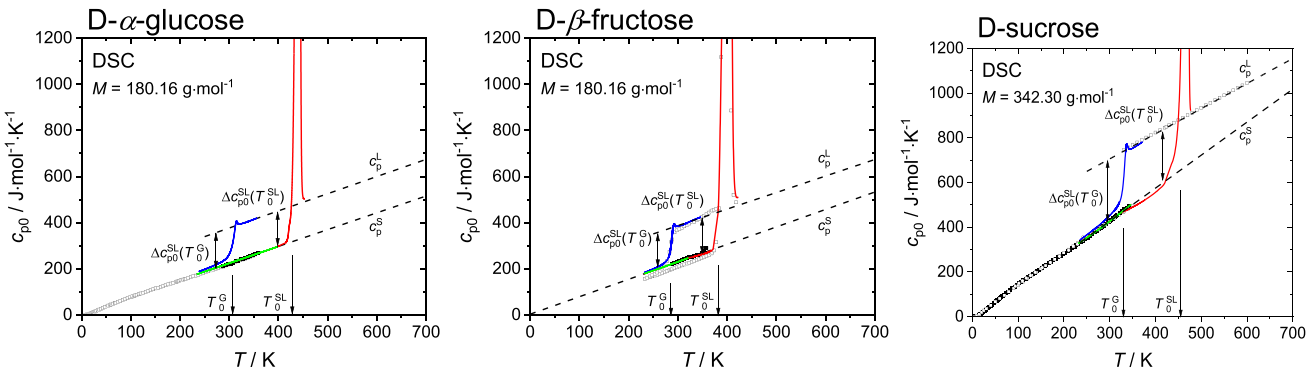

Fig. 4 Experimental specific heat capacity of crystalline (solid green line), phase transition from crystalline to liquid (solid red line) and glass transition (solid blue line) of (left) D-α-glucose, (middle) D-β-fructose and (right) D-sucrose by standard DSC. Literature data for D-α-glucose (solid black squares [43], empty black squares [44]), D-β-fructose (solid black squares [43], empty black squares [31]) and D-sucrose (solid black squares [45], empty black squares [33], empty black circles [46]) were also included. The results for D-α-galactose and D-α-xylose are in Figure S3 in SI

melting temperatures without introducing any correction for superheating. In future work, the possibility of superheating should be initially studied for similar compounds where melting occurs without decomposition (e.g. mannitol, erythritol).

It is important to point out that prior to melting properties investigation in wide scanning rate ranges, nowadays available with FSC, it was widely assumed that onset temperature and enthalpy determined from the endothermic peak from DSC, and several literature data signify the "*melting properties*". However, the "*melting properties*" determined in the non-linear dependency region cannot be explained in terms of thermal lag. Hence, this non-linear dependency is analyzed in terms of a chemical process by using isoconversional kinetics. Note that we refer to the

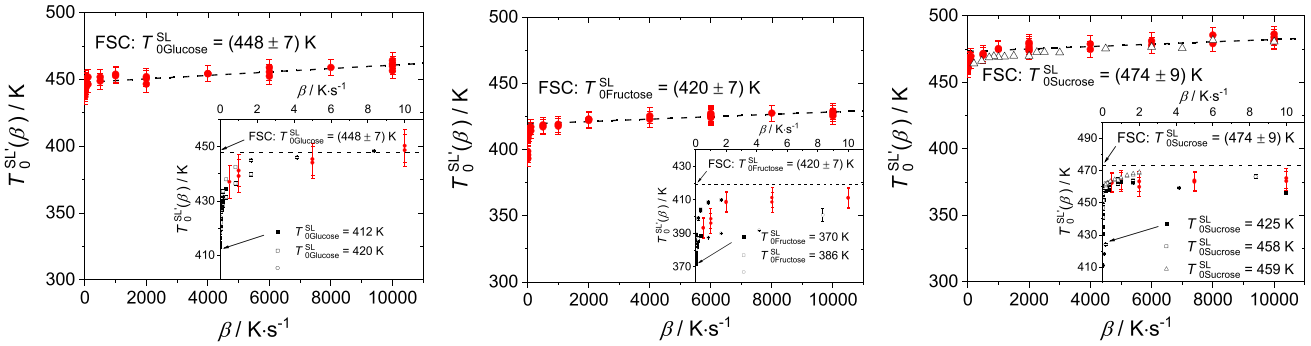

Fig. 5 Extrapolated onset temperature of the melting peak for (left) D-α-glucose, (middle) D-β-fructose and (right) D-sucrose determined from FSC (solid red circles) towards lower scanning rates. Literature data for D-α-glucose (solid black squares [32], empty black squares [27], empty black circles [47]), D-β-fructose (solid black squares [31], empty black squares [27], empty black circles [47]) and D-sucrose (solid black squares [33], empty black squares [27], empty black circles [47], empty black triangles [34]) were included for lower scanning rates

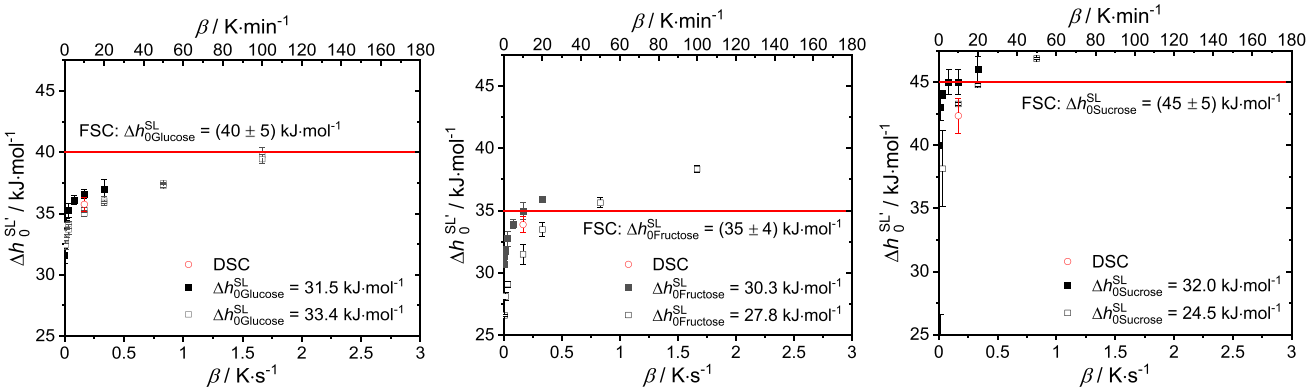

Fig. 6 Melting enthalpy for (left) D-α-glucose, (middle) D-β-fructose and (right) D-sucrose towards low scanning rates. Solid red lines indicate the melting enthalpy determined from FSC with higher scanning rates, as shown in Fig. 3, while empty red squares are melting enthalpy determined from DSC with 10 K·min^{-1}. Literature data for D-α-glucose (solid black squares [32], empty black squares [27]), D-β-fructose (solid black squares [31], empty black squares [27]) and D-sucrose (solid black squares [33], empty black squares [27]) were included for lower scanning rates

observed endothermic peak in the non-linear dependency region as a chemical process. We would like to highlight the distinction.

In terms of isoconversional kinetics [50], the conversion, α, was evaluated from the endothermic peak for heating rates in DSC and FSC measurements as

$$\alpha = \frac{\int_{t_0}^{t} \frac{dH}{dt} dt}{\int_{t_0}^{t_{total}} \frac{dH}{dt} dt} = \frac{\Delta H}{\Delta H_{total}} \quad (7)$$

where ΔH is the enthalpy of a segment of the endothermic peak and ΔH_{total} is the total enthalpy of the corresponding peak. The resulting temperature and heating rate dependence of the conversion are shown in Fig. 7.

Typically, with increasing scanning rates, the temperature dependence of the conversion shifts to higher temperatures. This was observed for D-α-glucose and D-β-fructose. However, this trend is not observed for low heating rates in D-sucrose. This could be explained by the application of too low heating rates for the FSC device together with a low thermal contact introducing additional uncertainty in temperature assessment of the conversion, α. Therefore, for D-sucrose, the temperature dependence of the conversion with very low heating rates was removed from consideration and only data for higher scanning rates but still < 1000 K·s^{-1} were used in the evaluation and are presented in Fig. 7(right).

By assuming an Arrhenius equation for the chemical process, the conversion rate corresponding to isoconversional conditions, α = const, at each heating rate was used to evaluate the apparent activation energy E_A and kinetic factor A for the chemical process, as an example of $\alpha = 0.2$ shown in Fig. 8.

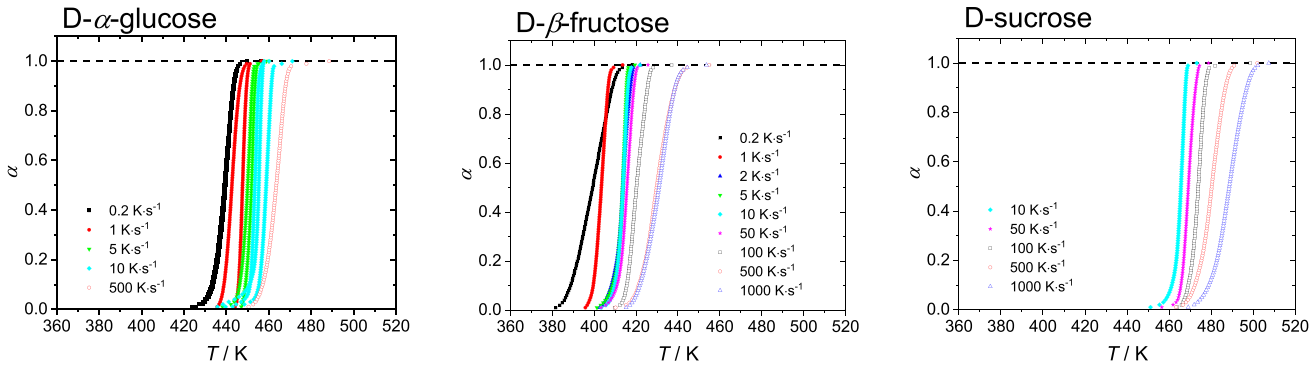

Fig. 7 Temperature dependence of the conversion for heating rate from 0.2 K·s^{-1} (10 K·min^{-1}) to 1000 K·s^{-1} for (left) D-α-glucose, (middle) D-β-fructose and (right) D-sucrose

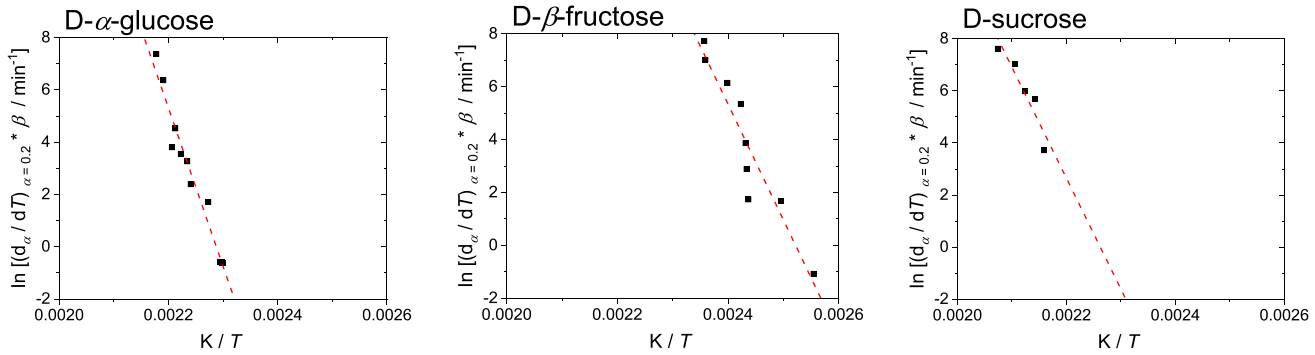

Fig. 8 Arrhenius plot of isoconversional at α = 0.2 for (left) D-α-glucose, (middle) D-β-fructose and (right) D-sucrose

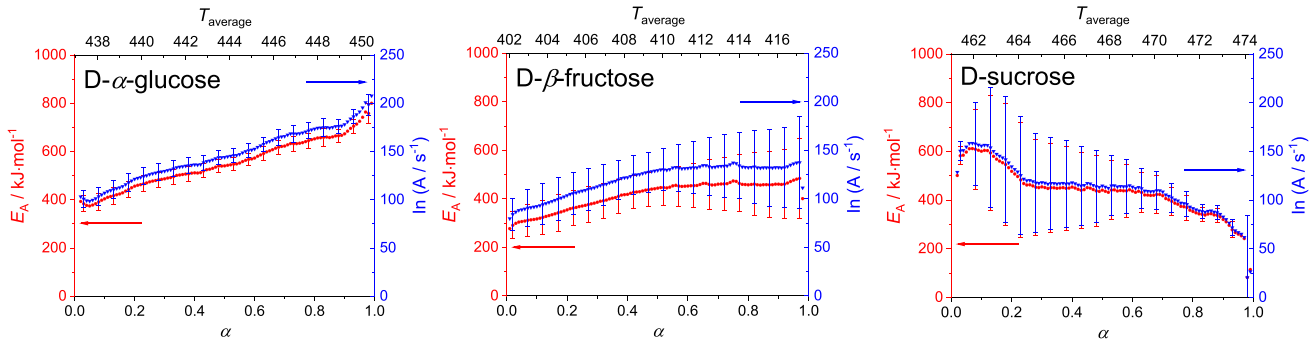

Fig. 9 The conversion dependence of activation energy, E_A and kinetic factor, A for the chemical process in (left) D-α-glucose, (middle) D-β-fructose and (right) D-sucrose. The uncertainty bars correspond to the standard deviation $k = 1$ and confidence level of 0.68

The conversional dependence of the activation energy E_A and A for different α of D-α-glucose, D-β-fructose, and D-sucrose are shown in Fig. 9.

PXRD Measurements The crystal structures of the initial solid state (as supplied) and the solid phase in equilibrium with the saturated solution were characterized with PXRD measurements to ensure the same crystal structure. In the knowledge of the mutarotation of the saccharides between the α-form and β-form in the liquid phase [51], the crystal structure diffractograms of the solid from the Cambridge Crystallographic Data Centre (CCDC) of the saccharide were compared to the measurements and presented in Fig. 10.

The pure D-glucose was characterized as D-α-glucose. In aqueous solutions, the formation of D-α-glucose

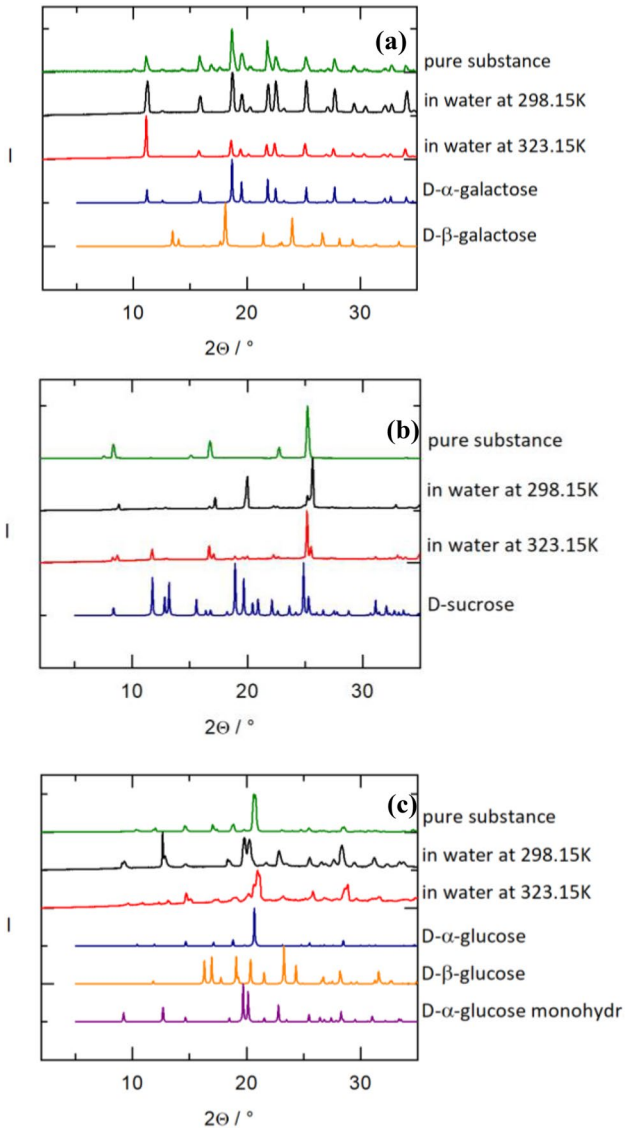

Fig. 10 PXRD diffractogram of (a) D-α-glucose, (b) D-sucrose and (c) D-α-galactose. Green line: pure substance; black line: solid phase of the supersaturated solution at $T = 298.15$ K, red line: solid phase of the supersaturated solution at $T = 323.15$ K, blue, orange and violet line: PXRD diffractograms from CCDC

monohydrate was observed at $T = 298.15$ K, which was already observed in the literature [52, 62]. The monohydrate was not found in solution at $T = 323.15$ K. This concludes that the dehydration temperature must be between 298.15 K and 323.15 K to form the anhydrous D-α-glucose. Furthermore, the diffractogram of the solid phase at $T = 323.15$ K shows similarities to the D-α-glucose and D-β-glucose diffractogram, which verifies the mutarotation in aqueous solutions.

For D-sucrose, D-β-fructose and D-α-xylose, and D-α-galactose no crystal change was observed in the solid phase during the solubility measurements. Therefore, D-β-fructose, D-α-xylose and D-α-galactose were assigned to their β-form and α-forms, respectively, and D-sucrose to the disaccharide crystal form α-glucopyranosyl-β-fructofuranoside. In this work, the PXRD measurements did not indicate crystal changes up to 323.15 K. In literature for even higher temperatures, solubility measurements were carried out, which means that the solubility literature data must be treated with care as to whether they are still valid for the higher temperatures. All the PXRD measurements are shown in Figure S4 in SI.

Solubility Modeling with PC-SAFT The solubility of all saccharides was modeled with PC-SAFT based on the experimental melting properties measured with FSC at rates > 1000 K·s^{-1}. The absolute relative deviations (ARD) is used to quantify the difference between PC-SAFT values and the experimental solubility according to Eq. (8)

$$\mathrm{ARD} = 100\frac{1}{NP}\sum_{k=1}^{NP}\left|\left(1-\frac{x_{\mathrm{k}}^{\mathrm{PC\text{-}SAFT}}}{x_{\mathrm{k}}^{\mathrm{exp}}}\right)\right| \tag{8}$$

where NP is the number of the available experimental solubility points, $x_{\mathrm{k}}^{\mathrm{exp}}$ and $x_{\mathrm{k}}^{\mathrm{PC-SAFT}}$ are the experimental solubility and PC-SAFT modeled solubility, respectively.

As already shown in the previous work [19], the $\Delta h_{0\mathrm{i}}^{\mathrm{SL}}$ has the most significant influence on the modeled solubility. Unfortunately, the melting enthalpies from FSC also show the highest uncertainty with up to 20% compared to 2% for $\Delta c_{\mathrm{p}_{0\mathrm{i}}}^{\mathrm{SL}}(T_{0\mathrm{i}}^{\mathrm{SL}})$ and 5% for $T_{0\mathrm{i}}^{\mathrm{SL}}$. Hence, the $T_{0\mathrm{i}}^{\mathrm{SL}}$ and the $\Delta c_{\mathrm{p}_{0\mathrm{i}}}^{\mathrm{SL}}(T_{0\mathrm{i}}^{\mathrm{SL}})$ were taken directly from the FSC measurement without varying within the experimental FSC uncertainty, while the melting enthalpy was adjusted within its FSC uncertainty to the experimental solubility data point at 298.15 K. In conclusion, the melting enthalpy adjusted by PC-SAFT is within the uncertainty of the FSC measurement for D-sucrose. For D-α-galactose the melting enthalpy was adjusted slightly outside the FSC uncertainty (Table 5) but still resulting in a good agreement between the PC-SAFT values and the experimental FSC data. The PC-SAFT parameters used in this work are listed in Table S1, while the single solubility diagram as well as the effect of the activity coefficients are shown and explained in Figures S5 and S6 in the SI. This shows that the effect of the mutarotation resulting in different solubilities as well as melting properties of the different crystal forms plays a crucial role in the solubility modeling of saccharides and needs to be further investigated.

Discussion

Melting Properties The experimental melting properties of saccharides have first been determined with FSC in a wide range of scanning rates from 2000 K·s^{-1} to 10,000 K·s^{-1}

Table 5 Solubility $w^{sat}_{298.15K}$ (uncertainties represents the standard deviations of multiple measurements, melting properties used in PC-SAFT: melting temperature T^{SL}_{0i}, melting enthalpy Δh^{SL}_{0i} and the slope ($a^{L}_{c_{p0i}}$, $a^{S}_{c_{p0i}}$) and interception ($b^{L}_{c_{p0i}}$, $b^{S}_{c_{p0i}}$) of the heat capacity of liquid and solid, and difference in the heat capacity at melting temperature $\Delta c^{SL}_{p0i}(T^{SL}_{0i})$

Substances	$w^{sat}_{298.15K}$ / g g^{-1}	T^{SL}_{0i} / K	Δh^{SL}_{0i} / kJ·mol^{-1}	$a^{L}_{c_{p0i}}$ / J·mol^{-1}·K^{-2}	$b^{L}_{c_{p0i}}$ / J·mol^{-1}·K^{-1}	$a^{S}_{c_{p0i}}$ / J·mol^{-1}·K^{-2}	$b^{S}_{c_{p0i}}$ / J·mol^{-1}·K^{-1}	$\Delta c^{SL}_{p0i}(T^{SL}_{0i})$ / J·mol^{-1}·K^{-1}
D-sucrose	0.6712 ± 0.05	474	49.52	1.167	328.995	1.516	-27.446	190.945
D-α-galactose	0.3256 ± 0.03	488	41.23	0.679	151.713	0.749	-4.192	121.618

and were then extended towards lower scanning rates from 1000 K·s^{-1} down to 1 K·s^{-1} for D-α-glucose, D-β-fructose, D-sucrose. The results were compared to the "*melting properties*" determined with DSC (0.17 K·s^{-1}; 10 K·min^{-1}), as well as literature data.

At first glance, the melting properties of D-α-glucose, D-β-fructose, and D-sucrose determined with the FSC technique are higher than literature data determined with DSC at rates ≤ 10 K·min^{-1}. The observed increase of the melting parameters with the heating rate reported in the literature were assessed to be due to three phenomena: (i) thermal lag resulting from the heat transfer in the calorimeter-sample system, (ii) chemical decomposition kinetics, and (iii) "superheating" [53–57]. Unfortunately, our data do not allow a separation of "superheating" from thermal lag and both effects are considered jointly. Superheating is a minor effect in our data since, within the uncertainty, a linear heating rate dependency is observed above 1000 K·s^{-1}.

In Fig. 5(right), the onset temperature of the melting peak in respect to scanning rates of D-sucrose determined with FSC in this work is in good agreement with literature FSC data by Toda et al. [34]. According to Toda, the melting temperatures measured with FSC from 0.5 K·s^{-1} to 10,000 K·s^{-1} were analyzed, including corrections to "superheating" and thermal lag, even though the melting temperatures decrease non-linearly with decreasing scanning rates below 1000 K·s^{-1} due to chemical processes. The equilibrium melting temperature was determined as T^{SL}_{0i} = 462.1 K by taking into consideration the non-linear region [34]. We strictly differentiate the regions with linear (above 1000 K·s^{-1}) and non-linear (below 1000 K·s^{-1}) scanning rate dependencies. The thermodynamic equilibrium melting temperature of D-sucrose determined in this work is T^{SL}_{0i} = (474 ± 9) K, not too far from the value reported by Toda [34].

Hence, the linear scanning rates dependency region (above 1000 K·s^{-1}) shown in Figs. 5 and 6 were attributed only to the thermal lag and accordingly corrected with extrapolation to zero scanning rate in order to obtain thermodynamic equilibrium melting properties.

The non-linear scanning rate dependency region (below 1000 K·s^{-1}) measured with FSC was also observed from literature data [27, 31–34, 48, 49], where the melting properties of saccharides have been intensively investigated.

Nevertheless, most literature studies concluded the equilibrium melting properties at zero scanning rate by considering the non-linear dependency. In the case of an unknown theoretical background of the observed phenomena and obvious non-linear dependency, such extrapolation can lead to errors in thermodynamic quantities, as shown below.

The non-linear region was analyzed with isoconversional kinetics in order to determine the type of observed process. As shown in Fig. 9 for D-α-glucose, D-β-fructose and D-sucrose, the activation energy at a level of 300–600 kJ·mol^{-1}, was observed for small conversions, α = 0.1 (at the start of the process). Such activation energy is higher than the sublimation enthalpy, e.g. the sublimation enthalpy of D-α-glucose is Δh^{SV}_{0i}(400 K) = (194 ± 5) kJ·mol^{-1} [58]. As generally agreed, no physical process can have an activation barrier higher than the lattice energy. The activation energy of 300–600 kJ·mol^{-1} can only be rationalized in terms of chemical kinetics corresponding to the decomposition of molecular compounds with dehydration, deamination, or decarboxylation processes within the crystal lattice [59, 60]. The same conclusion can be found in the work of Lee et al., who conducted a temperature modulated DSC study of melting/decomposition of D-sucrose combined with High-Performance Liquid Chromatographic analysis of the system at each treatment temperature [61], as well as in the work of Toda et al. [34]. The chemical decomposition has been noticed in other literature too. However, decomposition was commonly neglected and only considered as a small effect [27–33].

The decomposition of saccharides was also studied with TGA [31, 32]. The decomposition and corresponding mass loss were observed to occur above melting in the liquid phase. Additionally, in order to determine the stability of the saccharide,[32] very small mass losses of 2.5% and 3.5% were detected under isothermal conditions of 360 min at 413 K and 415 K, respectively. It has been concluded that the mass loss corresponds to dehydration of the saccharide and water evaporation.

The main question that arises from the isoconversional kinetic analysis of the FSC data is why the decomposition of D-α-glucose observed during non-isothermal TGA studies

occurs at higher temperatures (above the melting point) and has significantly lower activation energy.

Generally, saccharides have high solubility in water (74.1 g of D-α-glucose in 100 g of water at 373.15 K [62], and as it is assumed in most studies, the main product of saccharide decomposition at first stages is water. The high solubility or high interaction of water with the saccharide molecules in combination with a low concentration of water confined in the saccharide crystal lattice leads to a very low activity of water in saccharides. When the saccharide decomposes, the saccharide immediately dissolves in the decomposition product of water. Therefore, no mass loss can be determined experimentally at this temperature, and the temperature interval of mass loss determination is shifted significantly to higher temperatures, where the remaining saccharide is already liquid and the activity of water is significantly higher.

Solubility Modeling with PC-SAFT In the following, the solubility modeling is discussed. In Fig. 11 the aqueous temperature-dependent solubilities of D-sucrose and D-α-galactose are presented. In the literature, the isothermal method was mainly used to measure solubility applying different analytical methods (refractive index [3, 63], high-performance liquid chromatography [1, 9], gravimetric method [64]), which requires a sufficient time for the equilibration between the liquid and solid phase. The minimum equilibration time

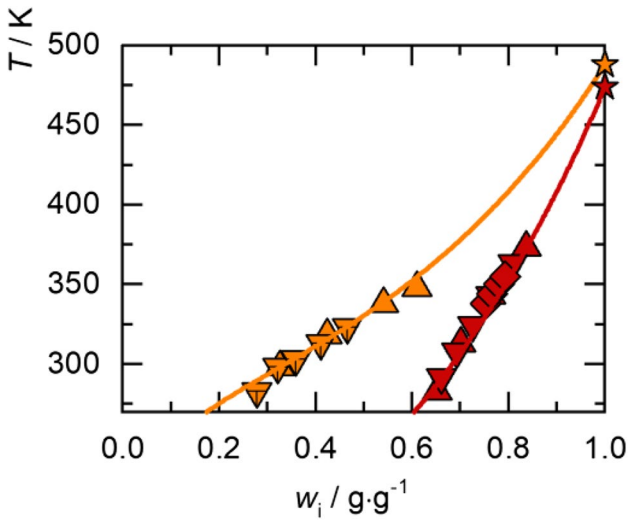

Fig. 11 The temperature-dependent weight-fraction based solubility w_i of D-sucrose and D-α-galactose: The symbols represent literature data, while the lines represent PC-SAFT modeling using PC-SAFT parameters from Table S1 in SI and melting properties from Table 2. D-sucrose: solid red up-triangles [3], solid red down-triangles [5], solid red diamonds [6], solid red line from PC-SAFT. D-α-galactose: solid orange up-triangles [7], solid orange down-triangles [65], solid orange line from PC-SAFT. The stars at $w_i = 1$ are the FSC derived melting temperatures from Table 2

is difficult to determine because the aqueous solutions are highly viscous due to the high solubility of the saccharides. Thus, the free mobility of the molecules is significantly restricted due to less free volume. Therefore, equilibrium times up to 48 h were chosen in the literature. It was also known that saccharides tend to decompose at higher temperatures (brown coloration due to the Maillard reaction). No brownish coloration was detected during the solubility measurements done in this work, so no decomposition due to the Maillard reaction took place.

The PC-SAFT modeling curves for the other compounds are not shown: Glucose forms a monohydrate in solution, so the modeling based on the melting properties of glucose anhydrate is not allowed based on Eq. 5. Fructose and xylose do not change crystal structure upon solubilizing the solid into the qeous solution. However, the PC-SAFT modeled melting enthalpy is not within the uncertainty of the FSC measured melting enthalpy, but it is clearly lower than the FSC value. For fructose a melting enthalpy of $\Delta h^{SL}_{0,Fructose,PC\text{-}SAFT} \approx 24 kJ/mol$ is obtained with PC-SAFT, while the FSC measurement yielded a minimum value of $\Delta h^{SL}_{0,Fructose,FSC,min} = 29 kJ/mol$. For xylose the same was observed ($\Delta h^{SL}_{0,Xylose,PC\text{-}SAFT} \approx 29 kJ/mol$ and $\Delta h^{SL}_{0,Xylose,FSC,min} = 37 kJ/mol$). This also shows that the results from PC-SAFT modeling do not correspond to either the DSC nor FSC measurement results. Therefore the modeling for these compounds was excluded from Fig. 11. The question to be answered is the origin of this deviation between FSC, DSC and PC-SAFT. One reason might be decomposition into chemically similar structures at higher temperatures. For D-α-glucose, different decomposition pathways are known, e.g. to erythrose + glycoaldehyde ($T^{SL}_{glycoaldehyde}$ = 370.15 K) [66] or glyceraldehyde ($T^{SL}_{glyceraldehyde}$ = 418.15 K) [60]. The lower melting temperatures indicate a high solubility of these compounds, which could explain the high measured solubility of D-α-glucose at high temperatures. Further, modeling is only allowed above the dehydration temperature of glucose, i.e. $T = 323.15$ K. This was already reported in literature resulting in the solubility order D-α-glucose monohydrate > D-α-glucose > D-β-glucose [63]. Another reason of the divergence between FSC and PC-SAFT is certainly tautomerism. The tautomeric equilibrium of the saccharides in aqueous solutions between the α-form and β-form in the pyranose or furanose form have been investigated in detail [51, 67]. Due to the mutarotation of monosaccharides in aqueous solution, over 99% of the pyranose form is found in solution [68], which contributes in the α-form (44%) and β-form (56%) for aqueous glucose solutions, respectively. In general, the solubility data of a compound has to end in its melting temperature in its pure

compound (cf, e.g. Figure 11). In the case of mutarotation, it is expected that the α-form and β-form have different crystal structures and thus different melting properties. As described before, the α-form shows higher solubility compared to the β-form of glucose. Therefore, the melting temperature of the α-form is also higher than that of the β-form. Since more D-β-glucose is in aqueous solutions, the literature solubility data tend to end in the melting temperature of D-β-glucose. The same phenomenon of mutarotation could be observed for the monosaccharides D-β-fructose and D-α-xylose. For D-α-galactose the solubility modeling was successful despite the fact that the mutarotation α-form (28.5%) and β-form (59.5%) was also reported in literature [69]. This can only be the case if the melting temperatures of the α-form and β-form are relatively close to each other. This has to be still investigated in the future. However, as shown in Fig. 11 the PC-SAFT modeled solubility based on experimental FSC result is in good agreement with experimental solubility and literature data for D-α-galactose.

To our best knowledge, for disaccharides such as D-sucrose mutarotation cannot be observed. In this work, D-sucrose solubility was modeled as previously done for amino acids [19, 20] and peptides [21, 22]. The FSC melting enthalpy was adjusted to the solubility at $T = 298.15$ K with the experimentally obtained difference between solid and liquid state heat capacities and is still within the FSC uncertainty. For D-scurose, other validations are possible: In the sugar industry, the following equation of Vavrinecz [70] is mainly used by sugar technologists to model the solubility of D-sucrose in water.

For T < 100 °C

$$\begin{aligned} w_{sucrose} &= 64.447 + 0.08222 \bullet T \\ &+1.6169 \bullet 10^{-3} \bullet T^2 \\ &-1.558 \bullet 10^{-6} \bullet T^3 \\ &-4.63 \bullet 10^{-8} \bullet T^4 \end{aligned} \quad (9)$$

For 100 °C < T < 140 °C

$$\begin{aligned} w_{sucrose} &= 71.0615 + 0.053625 \bullet T \\ &+6.55303 \bullet 10^{-4} \bullet T^2 \end{aligned} \quad (10)$$

where $w_{sucrose}$ is the solubility in $g_{D-sucrose} \bullet 100 g^{-1}_{solution}$ and T the temperature in °C. Since the model parameters in equations (9) and (10) were empirically adjusted to the solubility data, they show smaller deviations from the experimental solubility data compared to the PC-SAFT modeling, which is based purely on the experimentally determined melting properties of the pure substances. The pure-component parameters used in PC-SAFT are also fitted to non-solubility data (densities and osmotic coefficients in water). Nevertheless, the resulting PC-SAFT modelings are in good agreement with the experimental solubility and literature data (cf. Figure 11).

Conclusions

In this work, the melting properties of five saccharides (D-α-glucose, D-β-fructose, D-sucrose, D-α-galactose, and D-α-xylose) were successfully determined with FSC in a wide range of scanning rates from 1 $K \cdot s^{-1}$ up to 10000 $K \cdot s^{-1}$. The FSC results were compared to the "*melting properties*" determined with DSC (10 $K \cdot min^{-1}$), as well as literature data. The FSC results in the low scanning rate range agree well with the DSC results and the literature data. This validates the accuracy of the FSC measurement method. The scanning rate dependency of the melting properties (Figs. 5 and 6) can be divided into two regions, a linear dependency (above 1000 $K \cdot s^{-1}$) and a non-linear dependency (below 1000 $K \cdot s^{-1}$).

With FSC, the thermodynamic equilibrium melting temperatures of the saccharides were determined by extrapolating the apparent melting temperatures in the linear scanning rate dependency region (above 1000 $K \cdot s^{-1}$) to zero scanning rate, which corrects for the thermal lag and possible minor contributions from superheating.

In order to understand the chemical process contributing to the non-linear dependency (below 1000 $K \cdot s^{-1}$) regions, the melting peaks were analyzed in terms of isoconversional kinetics. The isoconversional method allows for the analysis of the scanning rate dependency of the melting properties. The activation energy determined from the kinetic analysis is higher than the sublimation enthalpy, and therefore the activation energies can only correspond to chemical decomposition, e.g. dehydration or deamination processes. This corresponds with the conclusion from Toda et al., where the "*melting*" kinetics of D-sucrose below the thermodynamic equilibrium melting temperature is mainly driven by decomposition kinetics [34]. This conclusion was also observed in the literature, though often disregarded in the determination of melting properties [27–32].

The experimental melting properties determined from FSC were used as input in PC-SAFT, resulting in successful modeling of solubility for D-sucrose. and D-α-galactose, which are in good agreement with the experimental solubility data and literature data. The solubility of D-α-glucose, D-β-fructose, and D-α-xylose cannot be modeled with PC-SAFT due to mutarotation. The effect of the mutarotation between the α-form and β-form plays an essential role in the solubility modeling and still needs to be further investigated.

It was shown that the experimentally determined melting properties are indispensable parts of solubility modelling using PC-SAFT. The access to the melting properties not only allows solubility modelling but also the quantification of the activity coefficients, which will give access

to future model validation. The combination of FSC and PC-SAFT opens the door to model solubility of solid compounds that decompose before melting.

Supplementary Information The online version contains supplementary material available at https://doi.org/10.1007/s11483-021-09707-6.

Acknowledgements The authors acknowledge funding from German Research Foundation (DFG) with Grants HE7165/6-1 and CH 1922/1-1. CS acknowledges financial support from the Ministry of Education and Science of the Russian Federation, grant 14.Y26.31.0019.

Funding Open Access funding enabled and organized by Projekt DEAL.

Declarations

Conflict of Interests There are no conflicts to declare.

References

1. M.C. Gray, A.O. Converse, C.E. Wyman, Sugar Monomer and Oligomer Solubility. Appl. Biochem. Biotech. **105–108**, 179–193 (2003)
2. L.A. Alves, J.B. Almeida e Silva, M. Giulietti, Solubility of d-Glucose in Water and Ethanol/Water Mixtures. J. Chem. Eng. Data **52**, 2166–2170 (2007)
3. C.E. Crestani, A. Bernardo, C.B.B. Costa, M. Giulietti, Fructose Solubility in Mixed (Ethanol + Water) Solvent: Experimental Data and Comparison among Different Thermodynamic Models. J. Chem. Eng. Data **58**, 3039–3045 (2013)
4. C. Held, G. Sadowski, A. Carneiro, O. Rodríguez, E.A. Macedo, Modeling thermodynamic properties of aqueous single-solute and multi-solute sugar solutions with PC-SAFT. AIChE J. **59**, 4794–4805 (2013)
5. W.S. Wise, E.B. Nicholson. Solubility and heats of crystallisation of sucrose and methyl glucoside in aqueoues solutions. J. Chem. Soc. 2714–2716 (1955)
6. M. Taylor, The solubility at high temperatures of pure sucrose in water. J. Chem. Soc. **1**, 1678–1683 (1947)
7. S.Ó. Jónsdóttir, S.A. Cooke, E.A. Macedo, Modeling and measurements of solid–liquid and vapor–liquid equilibria of polyols and carbohydrates in aqueous solution. Carbohyd. Res. **337**, 1563–1571 (2002)
8. A.M. Peres, E.A. Macedo, Measurement and Modeling of Solubilities ofd-Glucose in Water/Alcohol and Alcohol/Alcohol Systems. Ind. Eng. Chem. Res. **36**, 2816–2820 (1997)
9. X. Gong, S. Wang, H. Qu, Solid-Liquid Equilibria of D-Glucose, D-Fructose and Sucrose in the Mixture of Ethanol and Water from 273.2 K to 293.2 K. Chin. J. Chem. Eng. **19**, 217–222 (2011)
10. E.A. Macedo, A.M. Peres, Thermodynamics of ternary mixtures containing sugars. SLE ofd-Fructose in pure and mixed solvents. Comparison between Modified UNIQUAC and Modified UNIFAC. Ind. Eng. Chem. Res. **40**, 4633–4640 (2001)
11. A.M. Peres, E.A. Macedo, Phase equilibria of d-glucose and sucrose in mixed solvent mixtures: Comparison of UNIQUAC 1-based models. Carbohyd. Res. **303**, 135–151 (1997)
12. P. Tsavas, S. Polydorou, E.C. Voutsas, K.G. Magoulas, K. Naraghi, P.J. Halling, Sucrose Solubility in Mixtures of Water, Alcohol, Ester, and Acid. J. Chem. Eng. Data **47**, 513–517 (2002)
13. J.C. Givand, A.S. Teja, R.W. Rousseau, Effect of relative solubility on amino acid crystal purity. AIChE J. **47**, 2705–2712 (2001)
14. M. Sacchetti, Thermodynamics of water-solid interactions in crystalline and amorphous pharmaceutical materials. J. Pharm. Sci. **103**, 2772–2783 (2014)
15. D.M. Jiménez, Z.J. Cárdenas, D.R. Delgado, A. Jouyban, F. Martínez, Solubility and solution thermodynamics of meloxicam in 1,4-Dioxane and water mixtures. Ind. Eng. Chem. Res. **53**, 16550–16558 (2014)
16. M. Wesolowski, T. Konarski, General remarks on the thermal decomposition of some drugs. J. Therm. Anal. **43**, 279–289 (1995)
17. P. Cebe, X. Hu, D.L. Kaplan, E. Zhuravlev, A. Wurm, D. Arbeiter, C. Schick. Beating the heat-fast scanning melts silk beta sheet crystals. Sci. Rep. (2013)
18. P. Cebe, D. Thomas, J. Merfeld, B.P. Partlow, D.L. Kaplan, R.G. Alamo, A. Wurm, E. Zhuravlev, C. Schick, Heat of fusion of polymer crystals by fast scanning calorimetry. Polym. **126**, 240–247 (2017)
19. Y.Z. Chua, H.T. Do, C. Schick, D. Zaitsau, C. Held, New experimental melting properties as access for predicting amino-acid solubility. RSC Adv. **8**, 6365–6372 (2018)
20. H.T. Do, Y.Z. Chua, A. Kumar, D. Pabsch, M. Hallermann, D. Zaitsau, C. Schick, C. Held, Melting properties of amino acids and their solubility in water. RSC Adv. **10**, 44205–44215 (2020)
21. H.T. Do, Y.Z. Chua, J. Habicht, M. Klinksiek, M. Hallermann, D. Zaitsau, C. Schick, C. Held, Melting properties of peptides and their solubility in water. Part 1: dipeptides based on glycine or alanine. RSC Adv. **9**, 32722–32734 (2019)
22. H.T. Do, Y.Z. Chua, J. Habicht, M. Klinksiek, S. Volpert, D. Pabsch, M. Hallermann, M. Thome, D. Zaitsau, C. Schick et al., Melting properties of peptides and their solubility in water. Part 2: di- and tripeptides based on glycine, alanine, leucine, proline and serine. Ind. Eng. Chem. Res. **60**, 4693–4704 (2021)
23. A. Abdelaziz, D.H. Zaitsau, N.V. Kuratieva, S.P. Verevkin, C. Schick, Melting of nucleobases Getting the cutting edge of "Walden's Rule." Phys. Chem. Chem. Phys. **21**, 12787 (2019)
24. A. Abdelaziz, D.H. Zaitsau, T.A. Mukhametzyanov, B.N. Solomonov, P. Cebe, S.P. Verevkin, C. Schick, Melting temperature and heat of fusion of cytosine revealed from fast scanning calorimetry. Thermochim. Acta **657**, 47–55 (2017)
25. Y. Corvis, A. Wurm, C. Schick, P. Espeau, Vitreous State Characterization of Pharmaceutical Compounds Degrading upon Melting by Using Fast Scanning Calorimetry. J. Phys. Chem. B **119**, 6848–6851 (2015)
26. A. Magoń, A. Wurm, C. Schick, P. Pangloli, S. Zivanovic, M. Skotnicki, M. Pyda, Reprint of "Heat capacity and transition behavior of sucrose by standard, fast scanning and temperature-modulated calorimetry." Thermochim. Acta **603**, 149–161 (2015)

27. M. Hurtta, I. Pitkänen, J. Knuutinen, Melting Behavior of D-Sucrose, D-Glucose and D-Fructose. Carbohydr. Res. **339**, 2267–2273 (2004)
28. J.W. Lee, L.C. Thomas, S.J. Schmidt, Investigation of the heating rate dependency associated with the loss of crystalline structure in sucrose, glucose, and fructose using a thermal analysis approach (Part I). J. Agric. Food Chem. **59**, 684–701 (2011)
29. F. Örsi, Kinetic studies on the thermal decomposition of glucose and fructose. J. Therm. Anal. **5**, 329–335 (1973)
30. J. Fan, C.A. Angell, Relaxational transitions and ergodicity breaking within the fluid state: the sugars fructose and galactose. Thermochim. Acta **266**, 9–30 (1995)
31. A. Magoń, M. Pyda, Apparent heat capacity measurements and thermodynamic functions of D(-)Fructose by standard and temperature-modulated calorimetry. J. Chem. Thermodyn. **56**, 67–82 (2013)
32. A. Magoń, M. Pyda, Melting, glass transition, and apparent heat capacity of α-D-glucose by thermal analysis. Carbohyd. Res. **346**, 2558–2566 (2011)
33. A. Magoń, A. Wurm, C. Schick, P. Pangloli, S. Zivanovic, M. Skotnicki, M. Pyda, Heat capacity and transition behavior of sucrose by standard, fast scanning and temperature-modulated calorimetry. Thermochim. Acta **589**, 183–196 (2014)
34. A. Toda, R. Yamamura, K. Taguchi, T. Fukushima, H. Kaji, Kinetics of "Melting" of sucrose crystals. Cryst. Growth Des. **18**, 2602–2608 (2018)
35. S.M. Sarge, W. Hemminger, E. Gmelin, G.W.H. Höhne, H.K. Cammenga, W. Eysel, Metrologically based procedures for the temperature, heat and heat flow rate calibration of DSC. J. Therm. Anal. **49**, 1125–1134 (1997)
36. Netzsch. Thermal Decomposition of Glucose. https://www.netzsch-thermal-analysis.com/en/materials-applications/us-applications/thermal-decomposition-of-glucose/. Accessed 25 Sept 2021
37. Y.-Q. Chen, H.-B. He, C. Liu, X.-H. Lu. Thermal decomposition of glucose and sucrose by kinetics analysis. Chin. J. Process Eng. (2010)
38. F. Örsi, Kinetic studies on the thermal decomposition of glucose and fructose. J. Therm. Anal. **5**, 329–335 (1973)
39. S. van Herwaarden, E. Iervolino, F. van Herwaarden, T. Wijffels, A. Leenaers, V. Mathot, Design, performance and analysis of thermal lag of the UFS1 Twin-calorimeter chip for fast scanning calorimetry using the Mettler-Toledo flash DSC 1. Thermochim. Acta **522**, 46–52 (2011)
40. A. Abdelaziz, D.H. Zaitsau, T.A. Mukhametzyanov, B.N. Solomonov, P. Cebe, S.P. Verevkin, C. Schick, Melting temperature and heat of fusion of cytosine revealed from fast scanning calorimetry. Thermochim. Acta **657**, 47–55 (2017)
41. P. Cebe, D. Thomas, J. Merfeld, B.P. Partlow, D.L. Kaplan, R.G. Alamo, A. Wurm, E. Zhuravlev, C. Schick, Heat of fusion of polymer crystals by fast scanning calorimetry. Polymer **126**, 240–247 (2017)
42. J.M. Prausnitz, R.N. Lichtenthaler. *Molecular thermodynamics of fluid-phase equilibria* (1969)
43. G.O. Hernández-Segura, M. Campos, M. Costas, L.A. Torres, Temperature dependence of the heat capacities in the solid state of 18 Mono-, Di-, and Poly-Saccharides. J. Chem. Thermodyn. **41**, 17–20 (2009)
44. J. Boerio-Goates, Heat-capacity measurements and thermodynamic functions of crystalline a-D-Glucose at temperatures from 10 K to 340 K. J. Chem. Thermodyn. **23**, 403–409 (1991)
45. R.L. Putnam, J. Boerio-Goates, Heat-Capacity measurements and thermodynamic functions of crystalline sucrose at temperatures from 5 K to 342 K. Revised values for DfGm(sucrose, cr, 298.15 K), DfGm(sucrose, aq, 298.15 K), Sm(sucrose, aq, 298.15 K); and DrGm(298.15 K) for the hydrolysis of aqueous sucrose. J. Chem. Thermodyn. **25**, 607–613 (1993)
46. G.S. Parks, H.M. Huffman, M. Barmore, Thermal data on organic compounds. XI. The heat capacities, entropies and free energies of ten compounds containing oxygen or nitrogen. J. Am. Chem. Soc. **55**, 2733–2740 (1933)
47. J.W. Lee, L.C. Thomas, S.J. Schmidt, Can the thermodynamic melting temperature of sucrose, glucose, and fructose be measured using rapid-scanning Differential Scanning Calorimetry (DSC)? J. Agric. Food Chem. **59**, 3306–3310 (2011)
48. A. Raemy, T. Schweizer, Thermal behavior of carbohydrates studied by heat flow calorimetry. J. Therm. Anal. **28**, 95–108 (1983)
49. Y.H. Roos, Melting and glass transitions of low molecular weight carbohydrates. Carbohydr. Res. **238**, 39–48 (1993)
50. S. Vyazovkin, *Isoconversional kinetics of thermally stimulated processes* (Springer, 2015)
51. N. Le Barc, J.M. Grossel, P. Looten, M. Mathlouthi, Kinetic study of the mutarotation of D-glucose in concentrated aqueous solution by gas-liquid chromatography. Food Chem. **74**, 119–124 (2000)
52. G.L. Bockstanz, M. Buffa, C.T. Lira, Solubilities of alpha-anhydrous glucose in ethanol-water mixtures. J. Chem. Eng. Data **34**, 426–429 (1989)
53. J.W. Lee, L.C. Thomas, S.J. Schmidt, Effects of heating conditions on the glass transition parameters of amorphous sucrose produced by melt-quenching. J. Agric. Food Chem. **59**, 3311–3319 (2011)
54. B. Wunderlich, *Thermal analysis of polymeric materials* (Springer-Verlag, Berlin, 2005)
55. A.A. Minakov, A. Wurm, C. Schick, Superheating in linear polymers studied by ultrafast nanocalorimetry. Eur. Phys. J. E **23**, 43–53 (2007)
56. E.W. Hellmuth, B. Wunderlich, Superheating of linear high-polymer polyethylene crystals. J. Appl. Phys. **36**, 3039–3044 (1965)
57. M.C. Righetti, M.L. Di Lorenzo, Melting temperature evolution of non-reorganized crystals. Poly(3-Hydroxybutyrate). Thermochim. Acta **512**, 59–66 (2011)
58. V. Oja, E.M. Suuberg, Vapor pressures and enthalpies of sublimation of D-Glucose, D-Xylose, Cellobiose, and Levoglucosan. J. Chem. Eng. Data **44**, 26–29 (1999)
59. T.M. Aida, Y. Sato, M. Watanabe, K. Tajima, T. Nonaka, H. Hattori, K. Arai, Dehydration of d-glucose in high temperature water at pressures up to 80MPa. J. Supercrit. Fluids **40**, 381–388 (2007)
60. Y. Matsumura, S. Yanachi, T. Yoshida, Glucose decomposition kinetics in water at 25 MPa in the temperature range of 448–673 K. Ind. Eng. Chem. Res. **45**, 1875–1879 (2006)
61. J.W. Lee, L.C. Thomas, J. Jerrell, H. Feng, K.R. Cadwallader, S.J. Schmidt, Investigationof thermal decomposition as the kinetic process that causes the loss of crystalline structure in sucrose using a chemical analysis approach (Part II). J. Agric. Food Chem. **59**, 702–712 (2011)
62. L.A. Alves, J.B. Almeida e Silva, M. Giulietti, solubility of d-glucose in water and ethanol/water mixtures. J. Chem. Eng. Data **52**, 2166–2170 (2007)
63. F.E. Young, D-Glucose-water phase diagram. J. Phys. Chem. **61**, 616–619 (1957)
64. X. Gong, C. Wang, L. Zhang, H. Qu, Solubility of xylose, mannose, maltose monohydrate, and trehalose dihydrate in ethanol-water solutions. J. Chem. Eng. Data **57**, 3264–3269 (2012)
65. N.O. Shah, T.A. Nickerson, Functional properties of hydrolyzed lactose: solubility, viscosity and humectant properties. J. Food Sci. **43**, 1081–1084 (1978)
66. H. Michelsen, P. Klaboe, Spectroscopic studies of glycoaldehyde. J. Mol. Struct. **4**, 293–302 (1969)
67. L. Hyvönen, P. Varo, P. Koivistoinen, Tautomeric equilibria of D-glucose and D-fructose NMR spectrometric measurements. J. Food Sci. **42**, 657–659 (1977)

68. C.O. da Silva, B. Mennucci, T. Vreven, Density functional study of the optical rotation of glucose in aqueous solution. J. Org. Chem. **69**, 8161–8164 (2004)
69. T.M. Lowry, G.F. Smith, The mutarotation of galactose. J. Phys. Chem. **33**, 9–21 (1929)
70. G. Vavrinecz, Neue Tabelle über die Löslichkeit reiner Saccharose in Wasser. Z. Zuckerind. **87**, 481 (1962)

Authors and Affiliations

Yeong Zen Chua[1,2] · Hoang Tam Do[3] · Aarti Kumar[3] · Moritz Hallermann[3] · Dzmitry Zaitsau[2,4] · Christoph Schick[1,2,5] · Christoph Held[3]

Yeong Zen Chua
yeong.chua@uni-rostock.de

Christoph Schick
christoph.schick@uni-rostock.de

[1] Institute of Physics, University of Rostock, Albert-Einstein-Str. 23-24, 18051 Rostock, Germany

[2] Competence Centre CALOR, University of Rostock, Albert-Einstein-Str. 25, 18051 Rostock, Germany

[3] Laboratory of Thermodynamics, TU Dortmund University, Emil-Figge-Str. 70, 44227 Dortmund, Germany

[4] Institute of Chemistry, University of Rostock, Dr-Lorenz-Weg 2, 18051 Rostock, Germany

[5] Alexander Butlerov Institute of Chemistry, Kazan Federal University, 18 Kremlyovskaya Street, Kazan 420008, Russian Federation